

Variable Star Bulletin

Negative superhumps in the eclipsing Z Cam + VY Scl star ES Dra

Taichi Kato¹

tkato@kusastro.kyoto-u.ac.jp

¹ Department of Astronomy, Kyoto University, Sakyo-ku, Kyoto 606-8502, Japan

Received 2022 May 02

Abstract

I analyzed All-Sky Automated Survey for Supernovae (ASAS-SN) Sky Patrol data of ES Dra and classified it to be a Z Cam star with VY Scl-type fading episodes. An analysis of Transiting Exoplanet Survey Satellite (TESS) observations showed that this object shows shallow eclipses and that the orbital period is 0.17749895(17) d. Negative superhumps with a period of 0.167830(2) d and the beat phenomenon between the period of negative superhumps and the orbital period were detected in the TESS data between 2020 January and March. The orbital profile systematically varied depending on the beat phase and eclipses were missing in some phases. The eclipses in ES Dra were grazing and the disk was probably not eclipsed in some phases depending on the orientation of the tilted disk. These observations added a support to the interpretation of the precessing, tilted disk as the origin of negative superhumps. Negative superhumps disappeared 4 d before the VY Scl-type fading started. It was likely that the mass-transfer rate quickly dropped when negative superhumps disappeared and the decline of the total luminosity of the disk took 4 d. This provides a measurement of the time-scale of the response of the disk against a sudden decrease of the mass transfer in a VY Scl star. Although one of standstills in ES Dra was terminated by brightening, the identity of ES Dra as an IW And star would require further events.

1 Introduction

ES Dra was originally selected as a ultraviolet-excess object (PG 1524+622) and was confirmed to be a cataclysmic variable (CV) by spectroscopy (Green et al. 1986). The orbital period (P_{orb}) and the nature of this object has much been disputed. Andronov (1991) reported weak detections of the periods 1.07(8), 0.53(3) and 0.125(3) d. Andronov (1991) suggested a characteristic time-scale of 0.10–0.13 d. Although Ringwald (1993) suggested a spectroscopic orbital period of 0.179 d, it was finally published in Ringwald and Velasco (2012). Misselt and Shafter (1995) could not detect variations at the reported P_{orb} from observations on two nights. In the meantime, Tonny Vanmunster detected periods of 0.064(8) and 0.121(6) d during the 2001 June outburst.¹ Combined with observations by Jerry Foote, Vanmunster claimed to detect superhumps with a period of 0.1267(20) d and ES Dra was once considered as an SU UMa-type dwarf nova above the period gap. Baklanov et al. (2001) reported ~ 20 -d variations with an amplitude of 1.6 mag. Baklanov et al. (2001) suggested that the object is a novalike variable.

Ringwald and Velasco (2012) published a radial-velocity study giving $P_{\text{orb}}=0.17660(6)$ d and a spectral type of $M2\pm 1$ for the secondary. Ringwald and Velasco (2012) used American Association of Variable Star Observers (AAVSO) observations and concluded it to be a Z Cam star after the identification of standstills in 1995 and 2009. Simonsen et al. (2014) reached the same conclusion by showing a standstill in 2012 January to August.

¹<https://www.cbabelgium.com/cv_2001/Dra_ES_jun_2001.html>.

Table 1: Orbital period of ES Dra from TESS data

Interval BJD–2400000	TESS sector	Period (d)	Amplitude (mag)
58711–58737	S15	0.17746(4)	0.006
58738–58763	S16	0.17750(2)	0.015
58870–58982	S21–24	0.177491(8)	0.013
59419–59446	S41	0.17752(1)	0.014
59607–59636	S48	0.17749(2)	0.008

2 Long-term variation

I used All-Sky Automated Survey for Supernovae (ASAS-SN) Sky Patrol data (Shappee et al. 2014; Kochanek et al. 2017) and I confirmed that ES Dra is indeed a Z Cam star (vsnet-chat 8114).² Although the 2017 standstill was terminated by brightening (outburst), not by fading as in ordinary Z Cam stars (see e.g. Szkody and Mattei 1984), the importance of this finding was not recognized at that time. In 2020, I noticed two fading episodes (2019 August and 2020 April) in the ASAS-SN data and concluded that this object is a Z Cam + VY Scl star (vsnet-chat 8473).³ This classification has been adopted in AAVSO Variable Star Index (VSX: Watson et al. 2006). The long-term behavior based on the ASAS-SN data is shown in figures 1 and 2.

3 Orbital period and profile

I also analyzed Transiting Exoplanet Survey Satellite (TESS) observations (Ricker et al. 2015).⁴ The full light-curve is available at the Mikulski Archive for Space Telescope (MAST⁵). I used six high level science products (HLSP) sectors between 2019 August 15 and 2022 February 25 (figures 3, 4). I obtained P_{orb} for different states using the Phase Dispersion Minimization (PDM, Stellingwerf 1978) method after removing long-term trends by locally-weighted polynomial regression (LOWESS: Cleveland 1979). The errors of periods by the PDM method were estimated by the methods of Fernie (1989) and Kato et al. (2010). The results are shown in table 1. A PDM analysis of the entire segments as a whole did not yield a unique period. This was due to the variation of the orbital profile as discussed later. Shallow eclipses were seen following the orbital hump in S16, S21–24 and S48 and I obtained a unique period of 0.1774992(2) d after combination of these segments. The orbital period was refined using the Markov-Chain Monte Carlo (MCMC)-based method introduced in Kato et al. (2010). The resultant ephemeris is

$$\text{Min(BJD)} = 2459148.9510(7) + 0.17749895(17)E. \quad (1)$$

As will be shown later, this object showed negative superhumps between 2020 January and March and the orbital profile was variable depending on the presence/absence of negative superhumps. The mean orbital profiles in different states are shown in figure 5. When negative superhumps were completely absent, the orbital profile was that of a dwarf nova with a shallow eclipse showing an orbital hump at phase 0.8 (S16, S41 and S48). When negative superhumps were prominent, the hump moved to a different phase (S21–23 NSH). This result would, however, give a somewhat artificial impression since the amplitudes of negative superhumps were larger than those of orbital humps and the hump phase defined by P_{orb} may not be very adequate. This curve, however, indicates that the eclipses were present at the correct orbital phase even during the phase of negative superhumps and confirms the validity of P_{orb} determined in this study. This variation of the profile was the reason why a PDM analysis of the entire data set did not yield a unique P_{orb} . The S15 and S24 curves in this figure correspond to the epochs when the object experienced fading episodes (figure 2). It was most likely that the disk shrunk and eclipses disappeared. The orbital profile resembled that of ellipsoidal variation, consistent with a VY Scl star in low state.

²<http://ooruri.kusastro.kyoto-u.ac.jp/mailarchive/vsnet-chat/8114>.

³<http://ooruri.kusastro.kyoto-u.ac.jp/mailarchive/vsnet-chat/8473>.

⁴<https://tess.mit.edu/observations/>.

⁵<http://archive.stsci.edu/>.

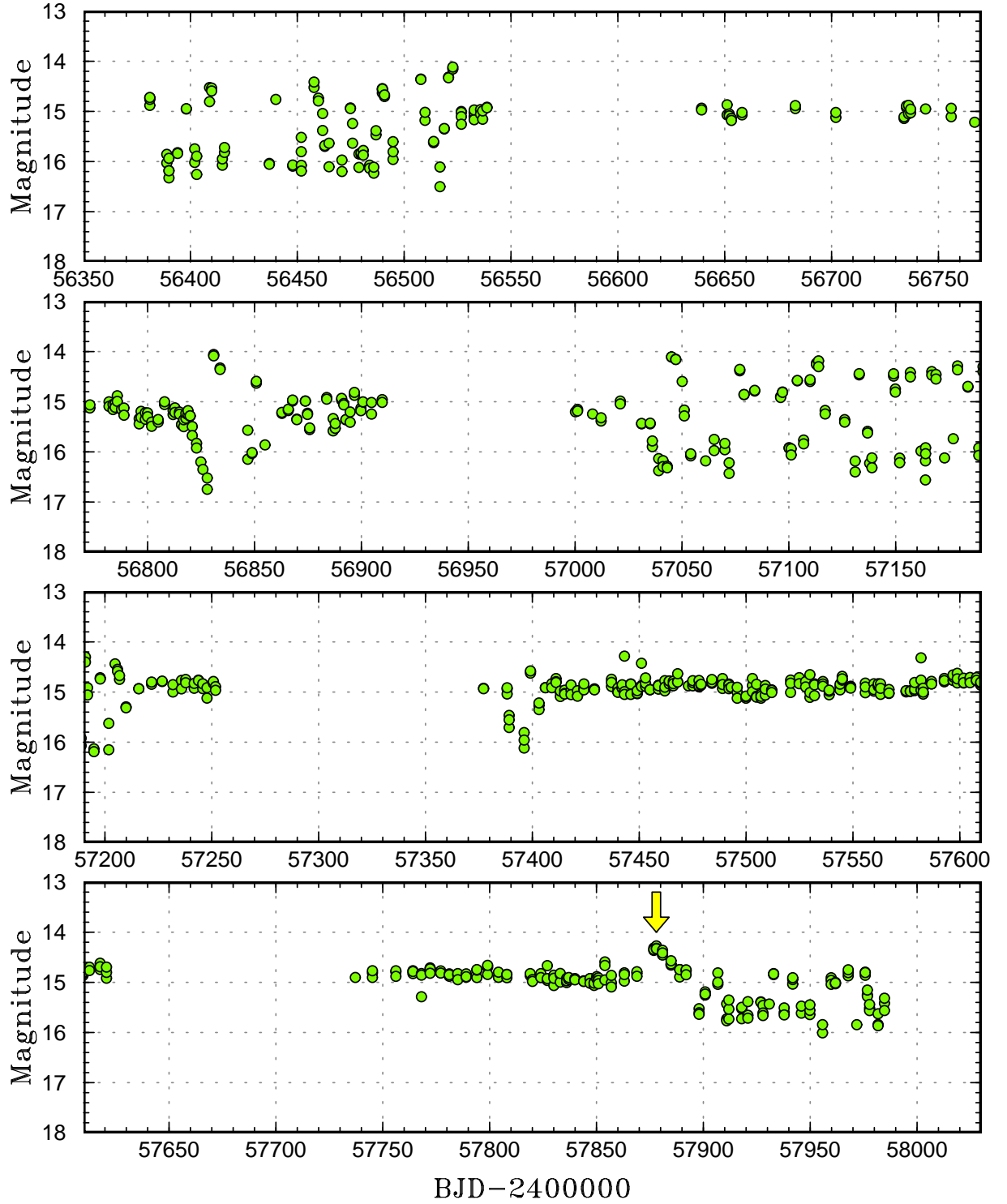


Figure 1: Long-term light curve of ES Dra using ASAS-SN V-band data (1). Both states with dwarf nova outbursts and standstills were recorded. The long standstill starting on BJD 2457406 was terminated by brightening (arrow in the fourth panel).

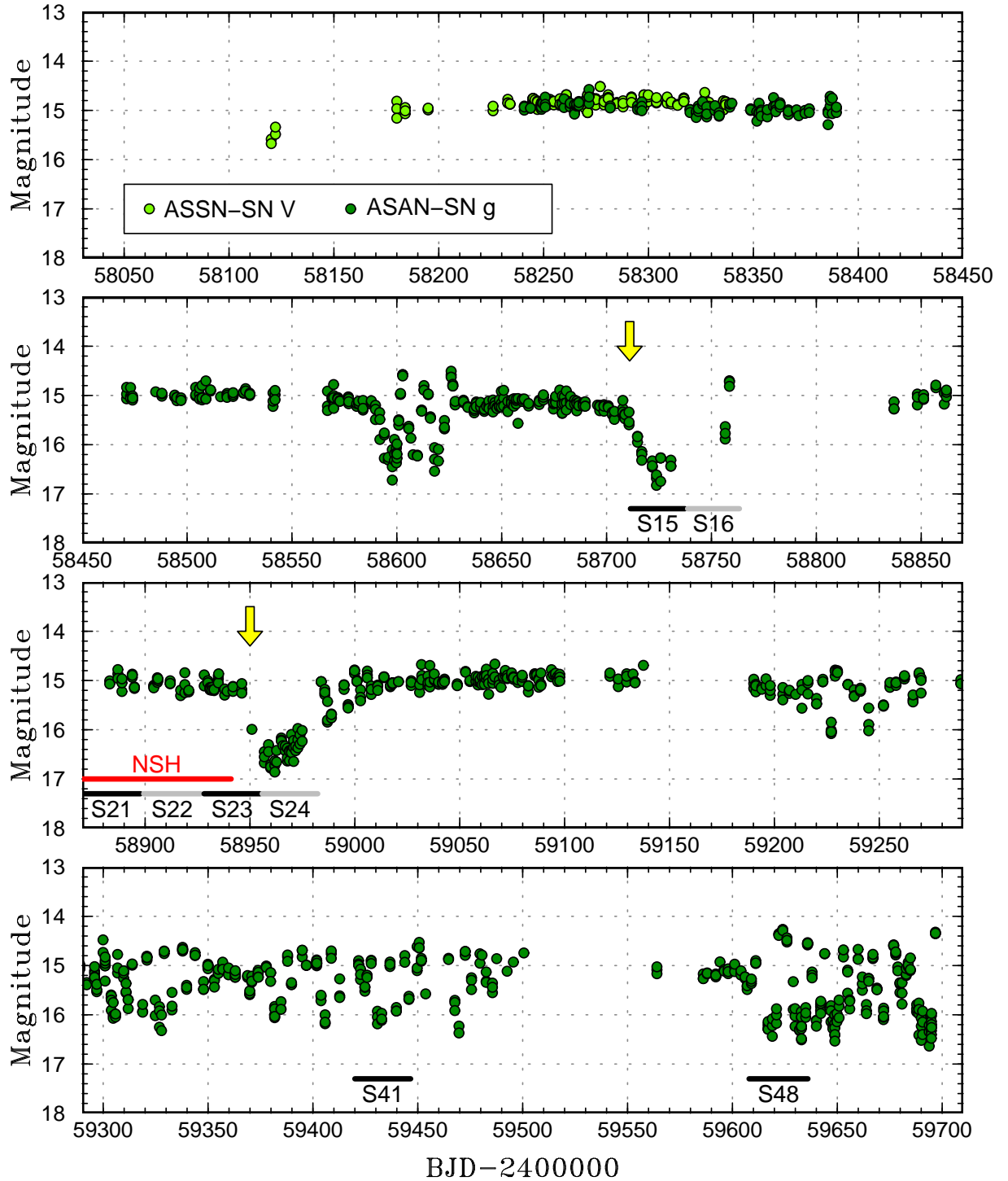


Figure 2: Long-term light curve of ES Dra using ASAS-SN data (2). Two fading episodes following standstills are shown by the arrows. The horizontal bars represent TESS sectors. The red horizontal bar represents the interval when negative superhumps (NSH) were present in the TESS data.

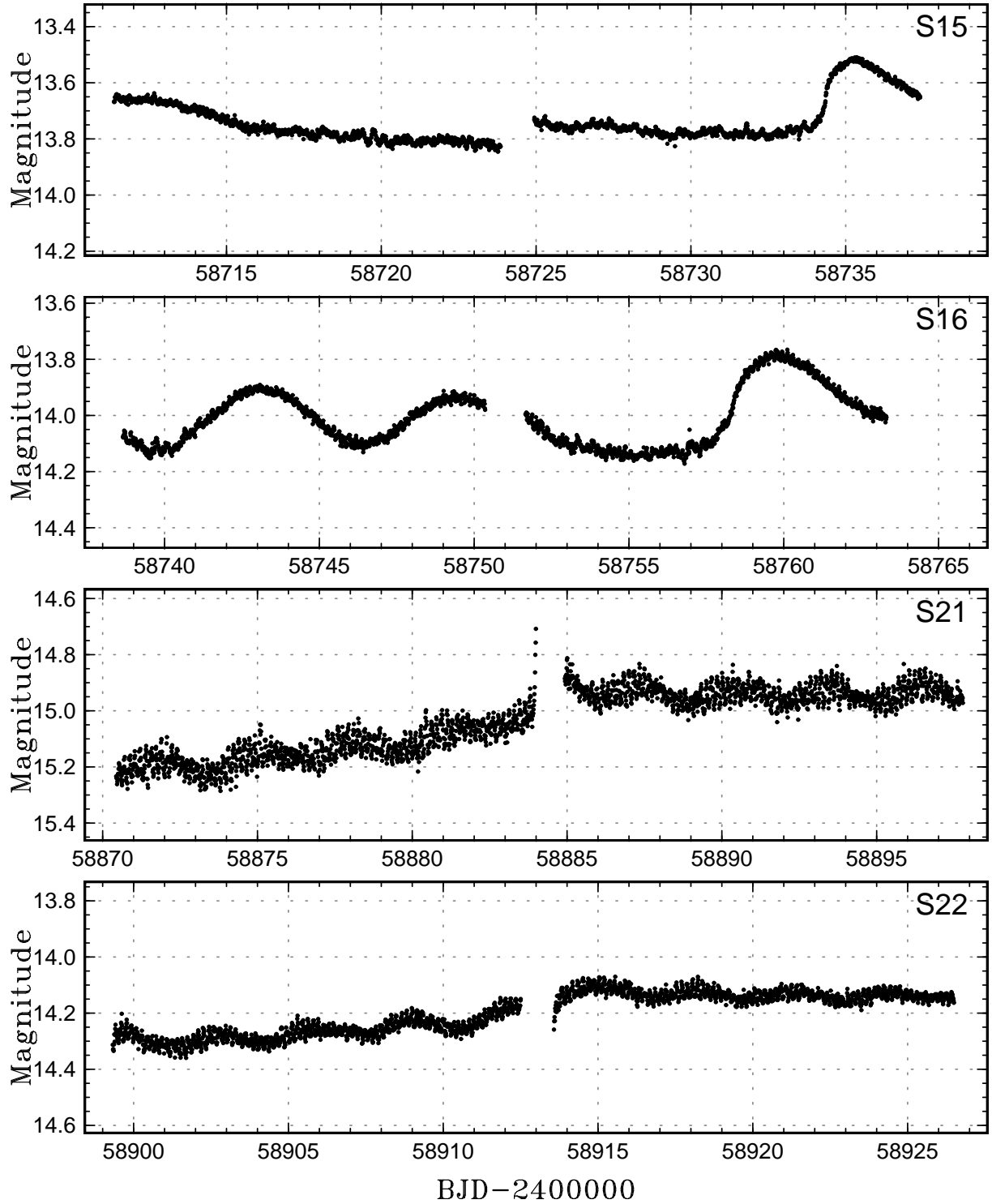


Figure 3: TESS light curve of ES Dra (1). The data were binned to 0.01 d. The numbers following S represent the TESS sector numbers. The magnitudes were defined as $-2.5 \log_{10}(\text{flux}/15000) + 10$. Beat phenomenon with a period of 3 d was present in S21 and S22.

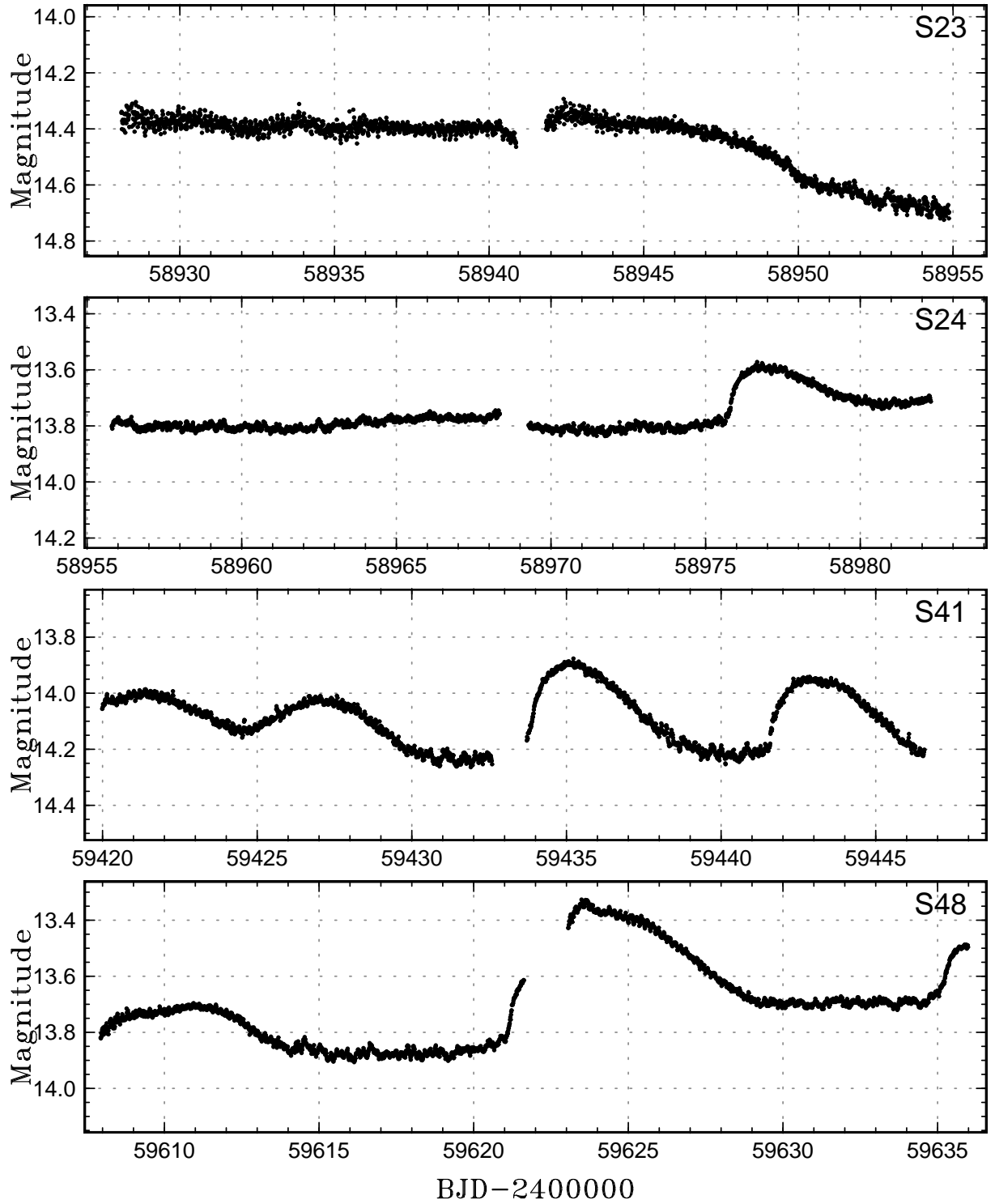


Figure 4: TESS light curve of ES Dra (2). See figure 3 for explanation.

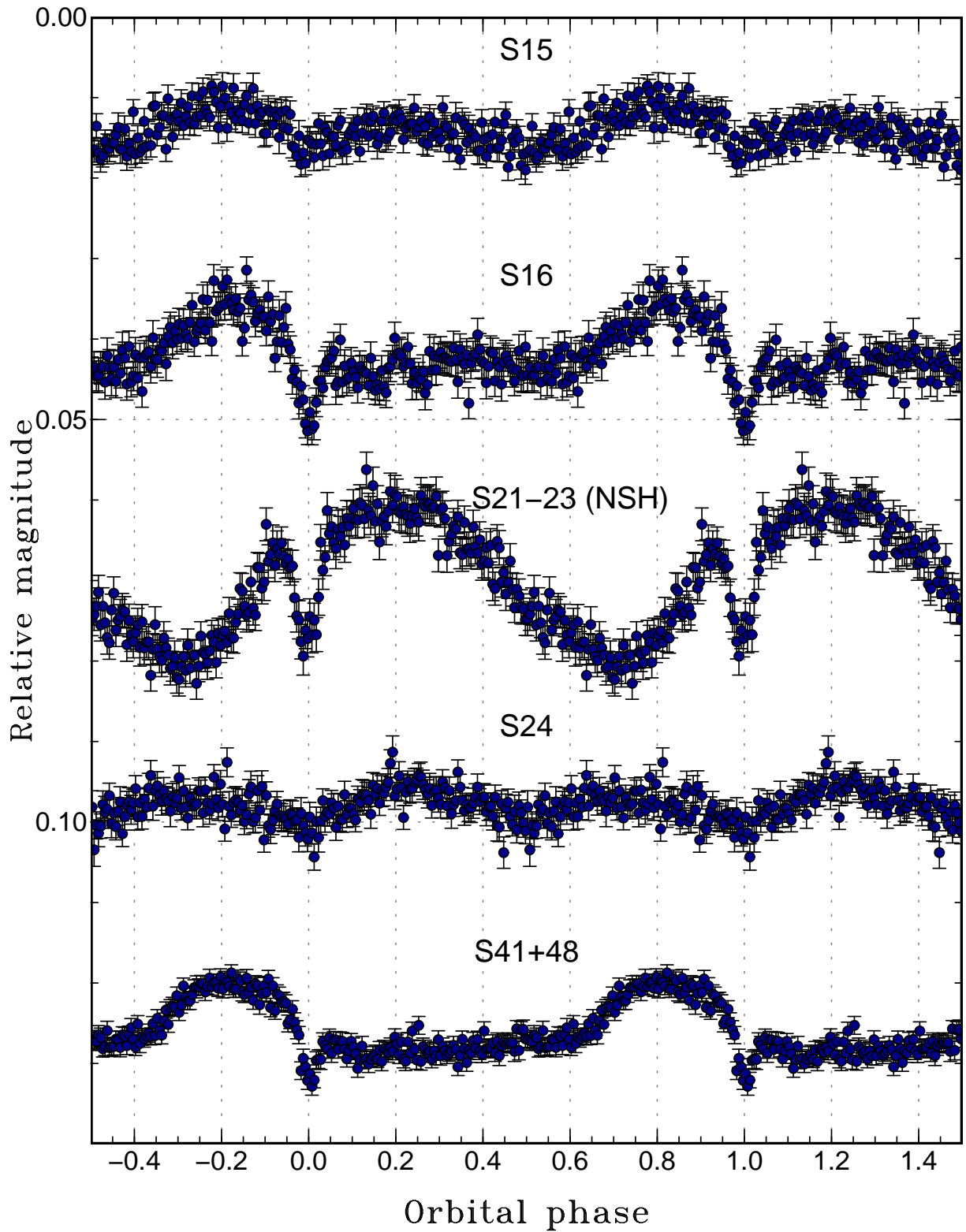


Figure 5: Mean orbital profiles of ES Dra. The ephemeris in equation (1) was used. The numbers following S represent TESS sector numbers (see figure 2). S21-23 (NSH) represents the interval when negative superhumps were detected. S24 includes a short segment of S23 when negative superhumps were absent.

4 Negative superhumps

A PDM analysis of the segment BJD 2458870–2458940 yielded a period of negative superhumps of 0.167830(2) d. The beat period with P_{orb} (3.08 d) is clearly visible in the TESS light curve (figure 6). The variation of orbital profiles depending on the beat phase (i.e. orientation of the disk to the observer assuming a tilted disk) is shown in figure 7. Although eclipses were present in most beat phases, they were not apparent for $\phi=0.50\text{--}0.75$.

The fractional superhump deficit for negative superhumps is $\epsilon^- = -5.4\%$, which is a typical value for this P_{orb} (Wood et al. 2009). It is widely believed that negative superhumps arise from the variable release of the potential energy when accreting on a precessing, tilted disk (Wood et al. 2000; Murray et al. 2002; Wood and Burke 2007). Recent detailed analysis of Kepler observations provided a strong support to this interpretation (Kimura et al. 2020; Kimura and Osaki 2021). ES Dra showed a clear beat phenomenon and this is also a support to the precessing, tilted disk as the origin of negative superhumps. A similar case has also been reported using TESS observations of LS Cam (Stefanov 2022; Rawat et al. 2022). Eclipses in ES Dra are grazing and the secondary only eclipses the outermost part of the disk. The absence of eclipses in for $\phi=0.50\text{--}0.75$ suggests that the part of the disk facing the secondary was most distant from the secondary when the secondary passes in front of the disk in this beat phase and was most difficult to eclipse. This variation of the eclipse depth depending on the beat phase also supports the precessing, tilted disk as the interpretation of negative superhumps.

The disappearance of negative superhumps when the object entered the low state was probably caused by the decrease of the mass-transfer rate. Negative superhumps disappeared 4 d earlier than the fading episode started (see figure 8). It was possible that the mass-transfer rate quickly dropped and the spot on the disk disappeared 4 d before the total luminosity of the disk started to decline.

5 System parameters and absolute magnitude

Assuming a standard Roche-filling secondary, the mass of the secondary (M_2) is expected to be $0.35M_{\odot}$ (Knigge 2006). The spectral type (M3.3) is in agreement with $M2\pm 1$ by Ringwald and Velasco (2012). The white dwarf in ES Dra is not expected to be particularly massive as judged from the absence of high excitation lines (Ringwald and Velasco 2012). Assuming an average-mass white dwarf ($M_1=0.81M_{\odot}$) for CVs (Pala et al. 2022), the mass ratio is expected to be $q = M_2/M_1 = 0.43$. The K_1 velocity of the primary is expected to be 112 km s^{-1} . Assuming that the disk of ES Dra in high state (in standstill) has a radius reaching the tidal truncation radius

$$r_{\text{tidal}} = \frac{0.60}{1+q}, \quad (2)$$

in unit of the binary separation (A) (Paczynski 1977), and assuming an optically thick standard disk, the observed eclipse could be best modelled by an inclination of $i=62.0\pm 0.5^\circ$. This value is most dependent on the disk radius and $i=64^\circ$ is the best for a disk radius of $0.38A$.

The K velocity of the emission ($K_{\text{em}}=134\pm 11 \text{ km s}^{-1}$) in Ringwald and Velasco (2012) is slightly larger than the value expected for these system parameters. If the emission line exactly traces the motion of the primary ($K_{\text{em}} = K_1 \sin i$), the best parameters are $M_1=0.53M_{\odot}$ and $i=61^\circ$. It is well-known that such an ideal case is rarely achieved, and we would better rely on the first solution until M_1 or q is independently measured.

Using Gaia EDR3 (Gaia Collaboration et al. 2021), the absolute magnitude M_V at standstill (in average) is $+5.7$ and peaks of dwarf nova outbursts reach $+4.9$. For an object with $i=61\text{--}64^\circ$, the effect of inclination

$$\Delta M_v(i) = -2.5 \log_{10} \left[\left(1 + \frac{3}{2} \cos i\right) \cos i \right], \quad (3)$$

is 0.19–0.35 mag. By adopting $i=62.0^\circ$, the corrected M_V for standstill and outburst peak are $+5.5$ and $+4.7$, respectively.

6 Standstill terminated by brightening

The phenomenon of a standstill terminated by brightening (outburst) in 2017 May is a signature of an IW And star (Simonsen 2011; Hameury and Lasota 2014; Kato 2019). As described in Kato (2019), typical IW And stars show a tendency of recurrence of this phenomenon which is frequently followed by a dip and subsequent damping oscillations. Such a cycle has not been yet apparent in ES Dra and it would be interesting to see whether this

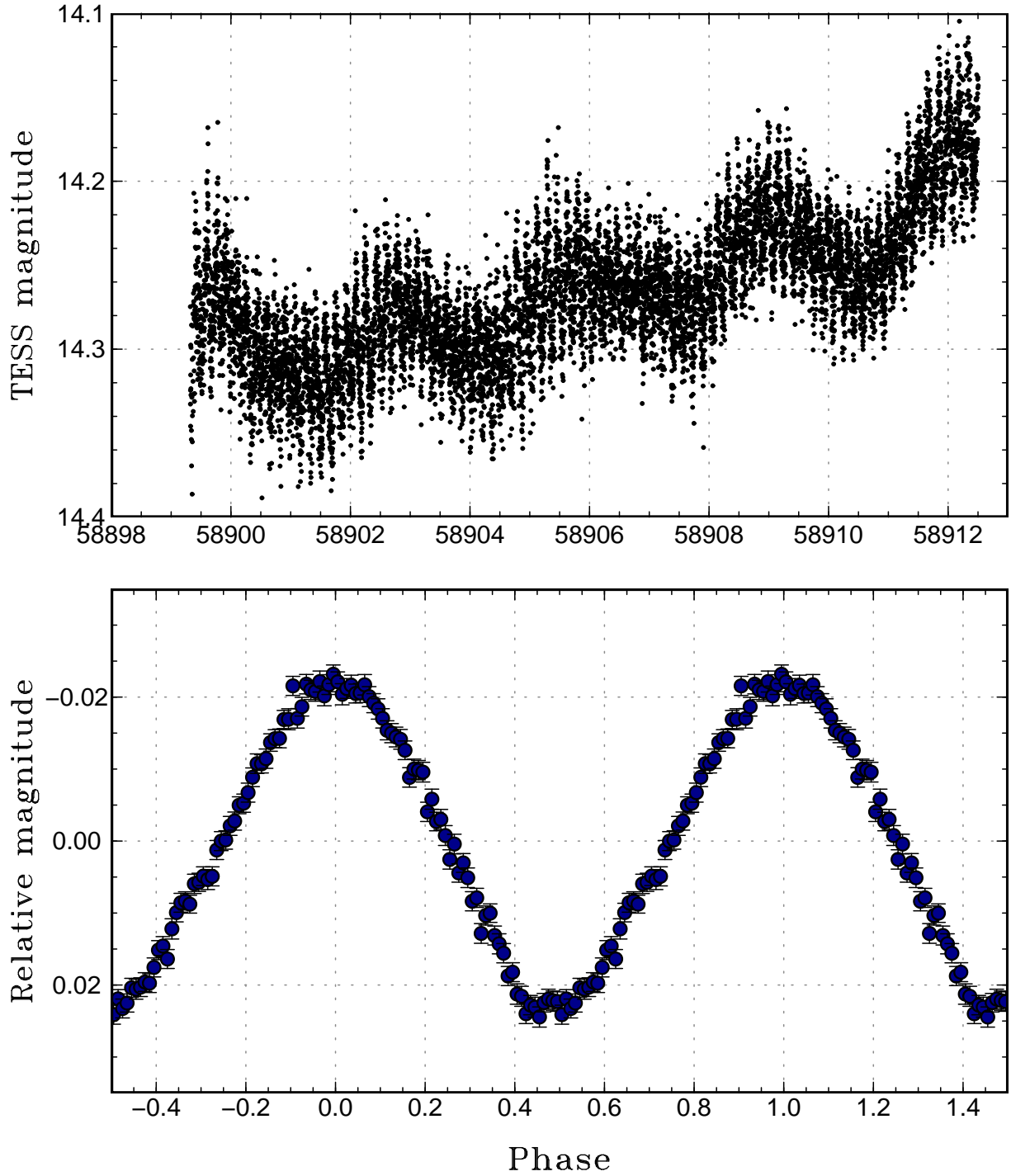


Figure 6: Negative superhumps in ES Dra. (Upper:) Example of TESS light curve. Both short-period modulations (negative superhumps) and the 3-d beat period were present. (Lower:) Profile of negative superhumps. The zero phase and the period were defined as BJD 2458905.118 and 0.167830 d, respectively.

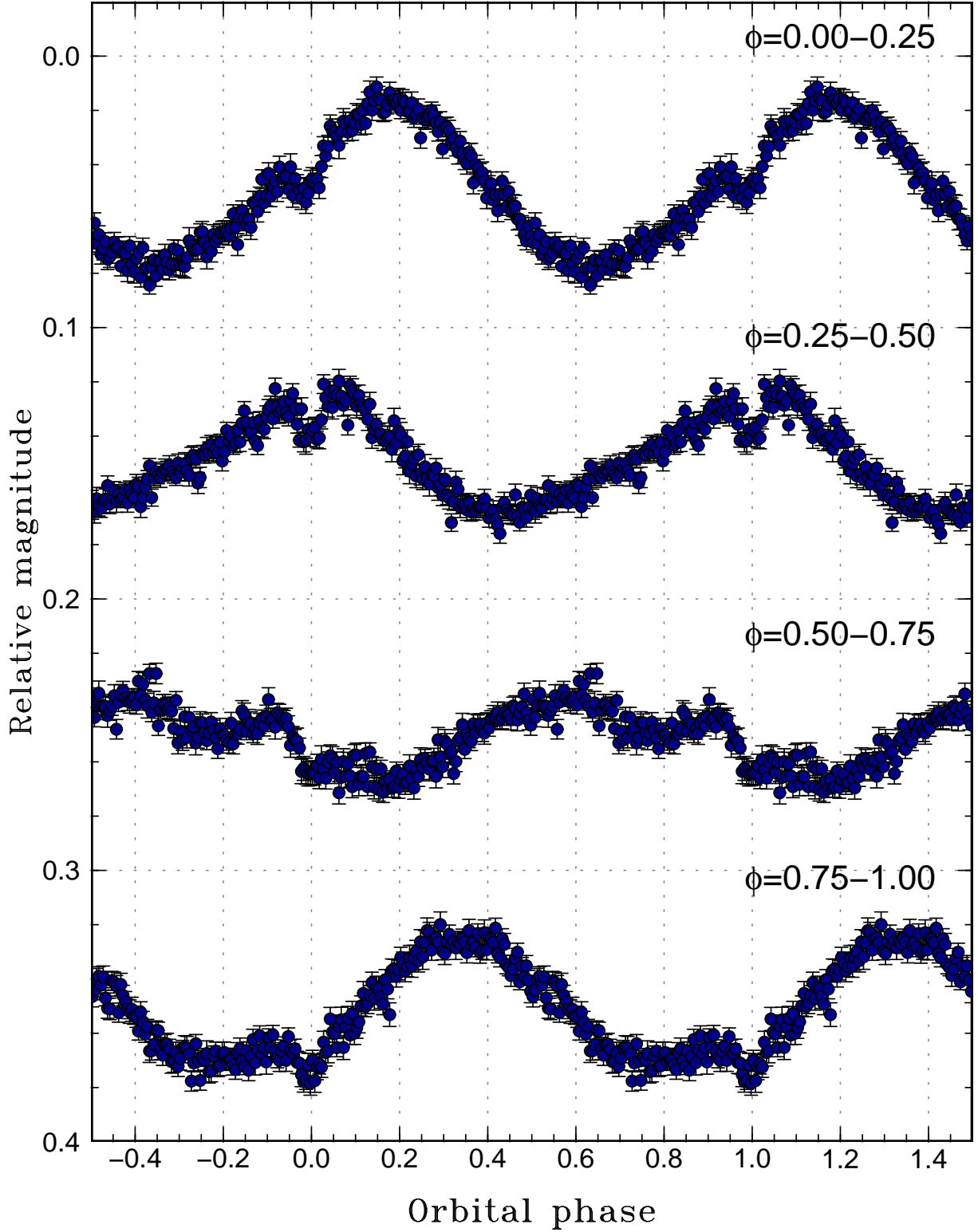


Figure 7: Variation of orbital profiles of ES Dra during the phase of negative superhumps. The beat phases ϕ were determined using the epoch of BJD 2458905.118 (see figure 6) and the beat period of 3.08096 d. The orbital phases were defined by equation (1).

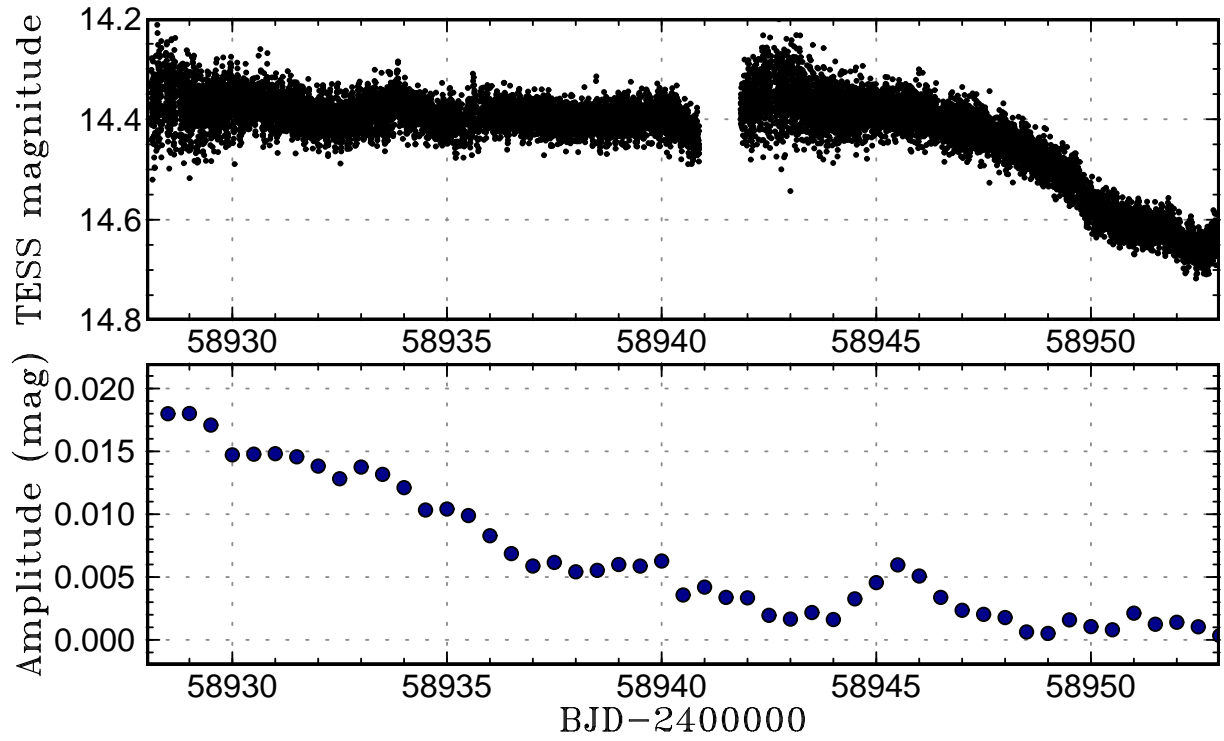


Figure 8: Light variation and amplitude of negative superhumps when ES Dra entered a VY Scl-type low state. (Upper:) TESS light curve. (Lower:) Amplitude of negative superhumps. The values were obtained for 3-d segments considering the beat phenomenon. The amplitude reached almost zero on BJD 2458943. The fading started on BJD 2458947.

object shows cyclic behavior in future as in typical IW And stars or the 2017 May event was a sporadic one and its resemblance to the IW And-type phenomenon was superficial.

Acknowledgements

This work was supported by JSPS KAKENHI Grant Number 21K03616. The author is grateful to the ASAS-SN and TESS teams for making their data available to the public. I am grateful to Naoto Kojiguchi for helping downloading the TESS data.

List of objects in this paper

IW And, Z Cam, LS Cam, ES Dra, SU UMa, VY Scl

References

- Andronov, I. L. (1991) Photographic observations of the cataclysmic variable candidates PG 1445+584 and PG 1524+622. *IBVS* **3645**, 1
- Baklanov, A. V., Pavlenko, E. P., & Dudka, O. I. (2001) CCD-fotometry of cataclysmic variable ES Dra in 2001. *Odessa Astron. Publ.* **14**, 24
- Cleveland, W. S. (1979) Robust locally weighted regression and smoothing scatterplots. *J. Amer. Statist. Assoc.* **74**, 829
- Fernie, J. D. (1989) Uncertainties in period determinations. *PASP* **101**, 225
- Gaia Collaboration et al. (2021) Gaia Early Data Release 3. Summary of the contents and survey properties. *A&A* **649**, A1
- Green, R. F., Schmidt, M., & Liebert, J. (1986) The Palomar-Green catalog of ultraviolet-excess stellar objects. *ApJS* **61**, 305
- Hameury, J.-M., & Lasota, J.-P. (2014) Anomalous Z Cam stars: a response to mass-transfer outbursts. *A&A* **569**, A48
- Kato, T. (2019) Three Z Cam-type dwarf novae exhibiting IW And-type phenomenon. *PASJ* **71**, 20
- Kato, T. et al. (2010) Survey of Period Variations of Superhumps in SU UMa-Type Dwarf Novae. II. The Second Year (2009-2010). *PASJ* **62**, 1525
- Kimura, M., & Osaki, Y. (2021) KIC 9406652: A laboratory for tilted disks in cataclysmic variable stars. II. Modeling of the orbital light curves. *PASJ* **73**, 1225
- Kimura, M., Osaki, Y., & Kato, T. (2020) KIC 9406652: A laboratory of the tilted disk in cataclysmic variable stars. *PASJ* **72**, 94
- Knigge, C. (2006) The donor stars of cataclysmic variables. *MNRAS* **373**, 484
- Kochanek, C. S. et al. (2017) The All-Sky Automated Survey for Supernovae (ASAS-SN) light curve server v1.0. *PASP* **129**, 104502
- Misselt, K. A., & Shafter, A. W. (1995) Time-resolved CCD photometry of a sample of Palomar-Green cataclysmic variable candidates. *AJ* **109**, 1757
- Murray, J. R., Chakrabarty, D., Wynn, G. A., & Kramer, L. (2002) Magnetically warped discs in close binaries. *MNRAS* **335**, 247
- Paczynski, B. (1977) A model of accretion disks in close binaries. *ApJ* **216**, 822

- Pala, A. F. et al. (2022) Constraining the evolution of cataclysmic variables via the masses and accretion rates of their underlying white dwarfs. *MNRAS* **510**, 6110
- Rawat, N., Pandey, J. C., Joshi, A., & Yadava, U. (2022) A step towards unveiling the nature of three cataclysmic variables: LS Cam, V902 Mon, and SWIFT J0746.3–1608. *MNRAS* **512**, 6054
- Ricker, G. R. et al. (2015) Transiting Exoplanet Survey Satellite (TESS). *J. of Astron. Telescopes, Instruments, and Systems* **1**, 014003
- Ringwald, F. A., & Velasco, K. (2012) The orbital period and variability of the dwarf nova ES Draconis. *New Astron.* **17**, 108
- Ringwald, F. A. (1993) PhD thesis Dartmouth Coll., Hanover, New Hampshire
- Shappee, B. J. et al. (2014) The man behind the curtain: X-rays drive the UV through NIR variability in the 2013 AGN outburst in NGC 2617. *ApJ* **788**, 48
- Simonsen, M. (2011) The Z CamPaign: Year 1. *J. American Assoc. Variable Star Obs.* **39**, 66
- Simonsen, M. et al. (2014) Z Cam stars in the twenty-first century. *J. American Assoc. Variable Star Obs.* **42**, 177
- Stefanov, S. Y. (2022) Unveiling the multiple periodicities of the cataclysmic variable LS Cam. *Bulgarian Astron. J.* **36**, 21
- Stellingwerf, R. F. (1978) Period determination using phase dispersion minimization. *ApJ* **224**, 953
- Szkody, P., & Mattei, J. A. (1984) Analysis of the AAVSO light curves of 21 dwarf novae. *PASP* **96**, 988
- Watson, C. L., Henden, A. A., & Price, A. (2006) The International Variable Star Index (VSX). *Society for Astronom. Sciences Ann. Symp.* **25**, 47
- Wood, M. A., Thomas, D. M., & Simpson, J. C. (2009) SPH simulations of negative (nodal) superhumps: a parametric study. *MNRAS* **398**, 2110
- Wood, M. A., & Burke, C. J. (2007) The physical origin of negative superhumps in cataclysmic variables. *ApJ* **661**, 1042
- Wood, M. A., Montgomery, M. M., & Simpson, J. C. (2000) Smoothed particle hydrodynamics simulations of apsidal and nodal superhumps. *ApJ* **535**, L39



This work is licensed under a Creative Commons “Attribution-NonCommercial-ShareAlike 4.0 International” license.

VSOLJ
c/o Keiichi Saijo National Science Museum, Ueno-Park, Tokyo Japan

Editor Seiichiro Kiyota
e-mail: skiyotax@gmail.com
